

Proximity effect in the presence of Coulomb interaction and magnetic field

P. M. Ostrovsky,^{1,2,*} Ya. V. Fominov,^{2,†} and M. V. Feigel'man^{2,‡}

¹*Institut für Nanotechnologie, Forschungszentrum Karlsruhe, 76021 Karlsruhe, Germany*

²*L. D. Landau Institute for Theoretical Physics RAS, 119334 Moscow, Russia*

(Dated: 9 February 2006)

We consider a small metallic grain coupled to a superconductor by a tunnel contact. We study the interplay between proximity and charging effects in the presence of the external magnetic field. Employing the adiabatic approximation we develop a self-consistent theory valid for arbitrary ratio of proximity and Coulomb strength. The magnetic field suppresses the proximity-induced minigap in an unusual way. We find the phase diagram of the grain in the charging energy – magnetic field plane. Two distinct states exist with different values and magnetic field dependences of the minigap. The first order phase transition occurs between these two minigapped states. The transition to the gapless state may occur by the first or second order mechanism depending on the charging energy. We also calculate the tunneling density of states in the grain. The energy dependence of this quantity demonstrates two different gaps corresponding to the Coulomb and proximity effects. These gaps may be separated in sufficiently high magnetic field.

PACS numbers: 74.45.+c, 74.50.+r, 73.21.-b

I. INTRODUCTION

A normal metal in contact with a superconducting lead acquires some superconducting properties; this phenomenon is known as the proximity effect (for review see, e.g., Ref. 1). In particular, the electron spectrum of the normal metal becomes gapped; at low interface transparency this gap is much smaller than superconducting Δ , hence the name minigap. This phenomenon is due to the Cooper pairs of the superconductor that penetrate into the normal metal and induce weak superconductive correlations there.

If a normal metal part of the superconductor – normal metal junction is a small grain then the Coulomb effects come into play (adding an electron to the grain costs charging energy). They are mostly pronounced in the tunneling experiment when the differential conductance between normal external tip and the small grain is measured (this quantity is proportional to what is called the tunneling density of states, TDOS). The Coulomb repulsion between tunneling electrons reduces the current. This phenomenon is known as tunneling anomaly or, in the zero-dimensional case, as Coulomb blockade.² Except the charging energy, an essential parameter governing the efficiency of the Coulomb blockade is the interface conductance G between the grain and the lead. In the case of normal lead the Coulomb blockade is developed² at $G \ll 1$ (we measure G in units of e^2/\hbar), and disappears³ at $G \gg 1$ due to the fact that an electron tunneling to the grain is rapidly transferred to the lead thus not blocking the tunneling of the next electron. At the same time, the Coulomb blockade persists even at $G \gg 1$ if the lead is superconducting because a single electron cannot escape into the lead due to the gap Δ in its single-particle density of states (DOS). This situation was studied by Matveev and Glazman.⁴

Apart from the tunnel current, the Coulomb interaction suppresses the proximity effect as well. The charg-

ing energy prevents Cooper pairs from tunneling to and from the normal grain and thus destroys the superconducting order induced on the normal side of the junction. Qualitatively, the Coulomb interaction is trying to fix the charge (neutrality) of the normal grain while the proximity effect fixes the phase. Charge and phase are conjugate variables obeying uncertainty principle: they may not be fixed simultaneously. Recently, the full quantitative description of this competition between the proximity and Coulomb effects in superconductor – normal metal junction at large interface conductance was derived in Ref. 5. Obviously, the Coulomb interaction diminishes the minigap. In this paper we extend the results of Ref. 5, including the external magnetic field into consideration. The magnetic field can easily be varied in experiment, and we demonstrate that the minigap is qualitatively sensitive to the strength of the magnetic field.

We consider a normal grain connected to a superconducting lead by tunnel junctions (low interface transparency) with large conductance G (determined by the product of transparency by the number of channels). We assume the zero-dimensional limit, i.e., the Thouless energy $E_{\text{Th}} = D/d^2$ is larger than all other relevant energy scales of the system including the superconductive gap Δ in the leads (here D is the diffusion constant in the grain and d is its characteristic size). In this limit, the proximity-induced minigap⁶ is $E_g = G\delta/4$, provided $E_g \ll \Delta$ and δ being the mean level spacing per one spin projection in the grain.

Our aim is to take into account effects of Coulomb interaction and magnetic field. The characteristic Coulomb energy $E_C = e^2/2C$ is assumed (similarly to Ref. 5) to lie in the same range as E_g :

$$\Delta \gg (E_g, E_C) \gg \delta. \quad (1)$$

The capacitance C of the grain already takes into account the renormalization $C = C_0 + e^2G/2\Delta$ due to virtual quasiparticle tunneling.⁷ This renormalization as-

sures the inequality $E_C \ll \Delta$ and allows arbitrary small geometric capacitance C_0 .

We consider relatively weak magnetic fields H that do not affect the superconducting lead, i.e., H should be much smaller than the critical field of the lead: $H \ll H_{c2} = \Phi_0/2\pi\xi_S^2$, where Φ_0 is the flux quantum and $\xi_S = \sqrt{D_S/\Delta}$ is the superconductive coherence length. Note that since the paramagnetic limit is much larger than H_{c2} , the condition $H \ll \Delta$ is certainly fulfilled (here and below we express H in the energy units dropping the factor $g\mu_B/2$).

If the normal grain is sufficiently small, we can neglect the orbital effect of the magnetic field in the grain. Indeed, as d decreases, the critical field due to orbital effects in a superconductor with the gap E_g , grows as $\Phi_0/\xi d$, where $\xi = \sqrt{D/E_g}$ is the coherence length corresponding to the proximity-induced superconductivity. At the same time, the Zeeman effect of the magnetic field determines the paramagnetic limit with the critical field of the order of E_g independent of the grain's size. Hence the disregard of the orbital effect is justified for small grains with $d \ll \Phi_0/\sqrt{DE_g}$.

To take into account both the proximity and charging effects, the adiabatic approximation was employed in Ref. 5. An inequality $E_C \gg \delta$ provides the separation of energy scales: electronic degrees of freedom (that are contained in the matrix Q of the sigma model, see below) are “slow” compared to the characteristic frequency of the electric potential fluctuations. This allows to calculate the renormalized (due to interaction) value of the minigap \tilde{E}_g . The result of the competition between charging and proximity effects is determined by the comparison of charging energy E_C with the effective “Josephson” energy $E_J \propto G^2\delta \log(\Delta/E_g)$. The latter has a clear meaning of the Josephson coupling energy⁸ between the superconductive reservoir and an imaginary weak superconductor with the order parameter E_g . The two limiting cases of the Coulomb vs. proximity competition are (i) *weak Coulomb blockade* limit, $E_J \gg E_C$, when small negative correction to the non-interacting minigap E_g arises, and (ii) *strong Coulomb blockade* regime, $E_J \ll E_C$, when the minigap is exponentially suppressed. The self-consistent approach allowing for the magnetic field is developed in Sec. II.

As we show below, the magnetic field does not influence the minigap \tilde{E}_g if $H < \tilde{E}_g/2$, while in the opposite case extra solutions of the model appear resulting in a rich phase diagram describing different possible values of the minigap. An extensive study of these solutions is presented in Sec. III.

The TDOS is also strongly affected by the magnetic field. This quantity is particularly interesting because it can be directly measured in the experiment as the differential conductance between the normal grain and a normal external tip, e.g., with the help of the tunnel microscopy technique. The Coulomb interaction produces a drastic impact on the TDOS: as the charging energy increases, the proximity minigap gradually transforms into

the Coulomb gap of the order of E_C . The magnetic field significantly changes the energy dependence of the TDOS due to the spin polarization of tunneling electrons. This effect is described in Sec. IV.

II. MODEL

Technically, we employ the replicated zero-dimensional σ model⁹ in imaginary time τ . This model is formulated for calculating the disorder average of the n th power (n is the number of replicas) of the partition function, $\langle \mathcal{Z}^n \rangle = \int e^{-S[Q,\phi]} DQ D\phi$. The standard coherent state functional-integral representation of the partition function¹⁰ deals with the action $S[\psi, \psi^*] = \psi^*(\partial_\tau - \mu)\psi + H[\psi^*, \psi]$ with ψ and ψ^* being fermionic anticommuting fields. The second-quantized Hamiltonian $H[\psi^*, \psi]$ contains the fourth-order term due to the Coulomb interaction. The disorder averaging induces another quartic term that mixes different replicas. These two terms are decoupled by the Hubbard-Stratonovich transformation with the help of a scalar variable ϕ_τ^a and a matrix field $Q_{\tau\tau}^{ab}$. These two objects are determined in the space of replicas and imaginary time (or, equivalently, Matsubara energies). As we are going to consider superconductive correlations, Q is also a 2×2 matrix in the Nambu-Gor'kov space. After the Hubbard-Stratonovich transformation, the action becomes quadratic in ψ and ψ^* and the Gaussian integration yields

$$\begin{aligned} S[Q, \phi] = & \frac{\pi\nu}{4\tau} \mathbf{Tr} Q^2 + \sum_a \int d\tau \frac{(\phi_\tau^a)^2}{4E_C} \\ & - \mathbf{Tr} \log \left[\xi - i\hat{\tau}_3(\varepsilon + iH) - i\phi - \frac{iQ}{2\tau} \right]. \end{aligned} \quad (2)$$

Here $\varepsilon = i\partial/\partial\tau$ is the Matsubara energy, $\hat{\tau}_i$ are the Pauli matrices in the Nambu-Gor'kov space, and ξ is the standard one-particle energy operator. The ‘ \mathbf{Tr} ’ symbol stands for the trace in all the three spaces of replicas, energies, and Nambu-Gor'kov, along with the integration in the real space. We assume the grain to be so small that the magnetic field has only Zeeman but not orbital effect. The zero-dimensional approximation also implies that both Q and ϕ do not vary in space and thus commute with ξ . The coupling of the grain to a superconductor will be described by a boundary term, which we will add to the action later.

The magnetic field lifts the degeneracy in the spin space. To account for this effect, one should derive the σ model with the twice larger Q matrix bearing also the spin indices. However, the correct result may be obtained directly from the model (2) with the help of the following trick. The only preferred direction in the spin space is fixed by the magnetic field. Thus the spin-dependent saddle-point Q matrix (we will use only its saddle-point value below) is block-diagonal and the action breaks up into two separate contributions from the

“up” and “down” spin states if the direction of the magnetic field is chosen as the spin quantization axis. Both these contributions are given by the action (2) but differ in the sign of the magnetic field. If a physical quantity calculated with the action (2) depends on the sign of H , one should simply take the average of the two values calculated at $\pm H$.

The σ model derivation proceeds with the expansion of the logarithm in Eq. (2) in soft modes of the Q field.¹¹ These modes are concentrated at small energies, $|\varepsilon| < 1/\tau$ with τ being the mean free time, and lie on the manifold $Q^2 = 1$. At higher energies the matrix is diagonal, $Q = \hat{\tau}_3 \operatorname{sgn} \varepsilon$. Before expanding the logarithm, we have to exclude high energy modes, associated with the fluctuations of the chemical potential, from the Q matrix. This is achieved by the gauge transformation¹²

$$Q_{\tau\tau'}^{ab} = e^{i\hat{\tau}_3 K_\tau^a} \tilde{Q}_{\tau\tau'}^{ab} e^{-i\hat{\tau}_3 K_{\tau'}^b}, \quad (3)$$

with properly chosen phase K_τ^a . The matrix $Q_{\tau\tau'}^{ab}$ depends on the two imaginary time indices and is *antiperiodic* on the interval $[0, 1/T]$. The gauge transformation may not alter these boundary conditions, thus we have to impose the restriction

$$K_{1/T}^a - K_0^a = 2\pi W^a, \quad (4)$$

with arbitrary integer W^a . For more rigorous calculation one also has to take into account the half-integer values of W^a . These values of the winding numbers imply that \tilde{Q} is *periodic* with respect to both imaginary time indices. The half-integer W^a are responsible for the parity effect.¹³ However, this effect is extremely weak in the proximity structure. To observe the parity effect, the two conditions should be fulfilled: (i) the minigap is of the order of E_C and (ii) the system is in the strong Coulomb blockade regime⁵ in which the “Coulomb staircase” is well pronounced. These two requirements are strongly inconsistent due to the large value of the junction’s conductance G . Thus hereafter we consider only integer W^a .

Assuming that \tilde{Q} contains only soft modes we expand the logarithm and obtain¹²

$$\begin{aligned} \mathcal{S}[\tilde{Q}, \phi] = & -\frac{\pi}{\delta} \operatorname{Tr} \left[((\varepsilon + iH)\hat{\tau}_3 + \phi - \dot{K})\tilde{Q} \right] \\ & + \sum_a \int d\tau \left[\frac{(\phi_\tau^a)^2}{4E_C} + \frac{(\phi_\tau^a - \dot{K}_\tau^a)^2}{\delta} \right]. \end{aligned} \quad (5)$$

Here the ‘Tr’ operation implies trace in all the three domains of the Q field. The last term of Eq. (5) comes from the logarithm expansion at energies well above $1/\tau$. It corresponds to the static compressibility of the electron gas. Thus we have to choose K such that $|\phi - \dot{K}|$ is minimized. The electric potential ϕ_τ^a is a real Bose field $\phi_\tau^a = T \sum_\omega \phi_\omega^a e^{-i\omega\tau}$. We separate the zeroth Fourier component into the integer and fractional part,

$\phi_{\omega=0}^a = 2\pi(W^a + w^a)$, and choose K_τ^a to be

$$K_\tau^a = C^a + 2\pi TW^a\tau - T \sum_{\omega \neq 0} \frac{\phi_\omega^a}{i\omega} e^{-i\omega\tau}. \quad (6)$$

The gauge transformation with such definition of the phase K was proposed in Ref. 14. Note, that we still have the freedom of adding an arbitrary time-independent constant C^a to K . Indeed, this will neither change $|\phi - \dot{K}|$ nor violate the restriction (4). The value of this constant will be fixed later after we add the boundary term to the action.

Now we can rewrite the action (5) in terms of K getting rid of the potential ϕ . Then the functional integration over ϕ is replaced by integration over K restricted by Eq. (4) along with summation over W and integration over w in the interval $[-1/2, 1/2]$. We also use the inequality $E_C \gg \delta$ and obtain

$$\begin{aligned} \mathcal{S}[\tilde{Q}, K] = & -\frac{\pi}{\delta} \operatorname{Tr} \left[((\varepsilon + iH)\hat{\tau}_3 + 2\pi Tw)\tilde{Q} \right] \\ & + 4\pi^2 T \sum_a \left[\frac{(w^a)^2}{\delta} + \frac{W^a w^a}{2E_C} \right] + \sum_a \int_0^{1/T} d\tau \frac{(\dot{K}_\tau^a)^2}{4E_C} \\ & - \frac{\pi G}{4} \operatorname{Tr} \left(Q_S e^{i\hat{\tau}_3 K} \tilde{Q} e^{-i\hat{\tau}_3 K} \right). \end{aligned} \quad (7)$$

Here we add the term that describes tunneling of electrons to and from the superconductive lead,¹¹ where the Q matrix takes the value

$$Q_S = 2\pi\delta^{ab}\delta(\varepsilon - \varepsilon')\hat{\tau}_1. \quad (8)$$

This form of Q_S is valid at low energies $\varepsilon \ll \Delta$. Below we consider various properties of the normal grain at energies not larger than E_g , thus the above approximation is suitable for our purposes. The high-energy contribution to the action (7) taking into account the energy dependence of Q_S , leads to the renormalization of the capacitance $C = C_0 + e^2 G/2\Delta$ as described in Ref. 7.

Throughout the paper we assume $T \gg \delta$. According to Eq. (7), this condition fixes $w^a = 0$ and leads us to the σ -model action

$$\begin{aligned} \mathcal{S} = & -\frac{\pi}{\delta} \operatorname{Tr} \left[(\varepsilon + iH)\hat{\tau}_3 \tilde{Q} \right] + \sum_a \int d\tau \left\{ \frac{(\dot{K}_\tau^a)^2}{4E_C} \right. \\ & \left. - \frac{\pi E_g}{\delta} \operatorname{tr} \left[\tilde{Q}_{\tau\tau}^{aa} (\hat{\tau}_1 \cos 2K_\tau^a + \hat{\tau}_2 \sin 2K_\tau^a) \right] \right\}, \end{aligned} \quad (9)$$

where ‘tr’ denotes the trace in the Nambu-Gor’kov space. In the absence of the magnetic field and the Coulomb interaction, the action (9) is the same as for the superconductive grain with the order parameter $E_g = G\delta/4$, therefore E_g plays the role of the bare minigap in our problem.⁶

Due to the condition $E_C \gg \delta$, we can employ the adiabatic approximation.⁵ Considering K as relatively “fast” variable in comparison with \tilde{Q} , we integrate the action

with respect to K at fixed \tilde{Q} . Then we come to the action for \tilde{Q} only and employ the saddle-point approximation. The simplest saddle point of that action is diagonal in replicas and Matsubara energies but not in the Nambu-Gor'kov space. Then the condition $\tilde{Q}^2 = 1$ may be explicitly resolved by the parameterization

$$\tilde{Q}_{\varepsilon\varepsilon'}^{ab} = 2\pi\delta^{ab}\delta(\varepsilon - \varepsilon') [\hat{\tau}_3 \cos \theta_\varepsilon^a + \hat{\tau}_1 \sin \theta_\varepsilon^a]. \quad (10)$$

The angle θ_ε is the standard Usadel angle.^{1,15} Generally, the \tilde{Q} matrix may also contain a $\hat{\tau}_2$ component that is not present in Eq. (10). This term, however, can always be eliminated by the proper choice of the constant C^a in the definition (6) of the phase K .

All eigenvalues of \tilde{Q} are ± 1 . In each replica and at every Matsubara energy we have a pair of $+1$ and -1 eigenvalues. Generally, the condition $\tilde{Q}^2 = 1$ admits arbitrary distribution of the eigenvalues' signs at small energies, $|\varepsilon| < 1/\tau$. However, the inequality $T \gg \delta$ allows to neglect these unconventional saddle points. This is provided by the very first term of the action (9), namely $-\pi\delta^{-1} \text{Tr}(\varepsilon\hat{\tau}_3\tilde{Q})$. The minimal Matsubara energy is πT , therefore the action of those saddle points is larger at least by $\pi^2 T/\delta$. The proximity effect, which is accounted for by other terms of the action, makes this estimate even stronger at low energies.

Substituting the ansatz (10) into Eq. (9), we find out that the action for K^a is local in imaginary time. This allows to describe the dynamics of K^a by the following Hamiltonian:

$$\hat{H}^a = E_C \left(-\frac{\partial^2}{\partial K^2} - 2q^a \cos 2K \right), \quad (11)$$

where the parameter q^a is determined by

$$q^a = \frac{\pi E_g}{2E_C\delta} \text{tr}(\hat{\tau}_1\tilde{Q}_{\tau\tau}^{aa}) = \frac{E_g}{2E_C\delta} \int_{-\Delta}^{\Delta} d\varepsilon \sin \theta_\varepsilon^a. \quad (12)$$

We cut off the logarithmically divergent integration at Δ since the expression (8), that we used for Q_S , is valid only at $\varepsilon \ll \Delta$. The dynamics of K is restricted by the condition (4). The summing over all integer W^a results in the periodic boundary conditions for the eigenfunctions of the Hamiltonian (11) on the interval $[0, 2\pi]$. This Hamiltonian has an important symmetry: it commutes with the transformation $K \mapsto K + \pi$. This is related to the conservation of the electron parity in the grain. The electron number operator is $\hat{n} = -i\partial/\partial K$. In this representation the first term of the Hamiltonian (11) is diagonal while the second one can change n by ± 2 only. Physically, this property is the consequence of the Andreev reflection mechanism that changes the charge by $\pm 2e$. Another symmetry of the Hamiltonian (11) is the inversion: $K \mapsto -K$. This is due to the particle-hole symmetry. It can be lifted by an external gate, which we do not consider in this paper.

Throughout the paper we assume that the temperature lies in the range

$$\delta \ll T \ll \tilde{E}_g. \quad (13)$$

The upper bound allows to replace all sums over the Matsubara energies by the corresponding integrals as it was done in Eq. (12). The adiabatic approximation relies on the fact⁵ that the characteristic frequency of the phase K fluctuations is much larger than \tilde{E}_g . At temperatures under discussion, K is frozen in the ground state of the Hamiltonian (11) with the energy $E_0(q) = E_C a_0(q)$, where $a_0(q)$ is the zeroth Mathieu characteristic value. The effective action for the \tilde{Q} matrix in terms of the angle θ is then

$$S = \sum_a \int d\tau \left[-\frac{1}{\delta} \int d\varepsilon (\varepsilon + iH) \cos \theta_\varepsilon^a + E_0(q^a) \right]. \quad (14)$$

The fact that the action is represented as a sum of independent identical contributions from each replica, is due to the trivial in replicas ansatz (10). The next step is the saddle-point approximation. The specific form of the action (14) implies that the saddle-point value of angle θ is independent of replica index. Using this fact we omit all replica indices hereafter.

The variation of Eq. (14) gives $\tan \theta_\varepsilon = \tilde{E}_g/(\varepsilon + iH)$, where the constant \tilde{E}_g is determined by the system of the self-consistency equations:

$$\frac{\tilde{E}_g}{E_g} = -\frac{1}{2E_C} \frac{\partial E_0}{\partial q}, \quad q = \frac{E_g \tilde{E}_g}{E_C \delta} \log \frac{2\Delta}{\Omega(\tilde{E}_g, H)}. \quad (15)$$

Here we introduce the notation

$$\Omega(\tilde{E}_g, H) = \max(\tilde{E}_g, H) + \sqrt{\max^2(\tilde{E}_g, H) - \tilde{E}_g^2}. \quad (16)$$

The last of Eqs. (15) is obtained from Eq. (12) where the found value of angle θ_ε was substituted.

The parameter \tilde{E}_g has the meaning of the renormalized minigap in the thermodynamic density of states for one spin subband. The thermodynamic DOS itself (for spin up) is obtained from \tilde{Q} after the analytic continuation to the real energy E in the following way:

$$\rho_\uparrow(E) = \frac{1}{\delta} \text{Re} \text{tr} \hat{\tau}_3 \tilde{Q}_{\varepsilon\varepsilon} \Big|_{\varepsilon \rightarrow -iE+0}. \quad (17)$$

As a result, it acquires the standard BCS form shifted by H (while the DOS for the spin down, ρ_\downarrow , is shifted by $-H$). The total DOS is

$$\rho(E) = \frac{1}{2} [\rho^{\text{BCS}}(E + H) + \rho^{\text{BCS}}(E - H)], \quad (18)$$

$$\rho^{\text{BCS}}(E) = \frac{2}{\delta} \text{Re} \cos \theta_\varepsilon \Big|_{\varepsilon \rightarrow -iE+0} = \frac{2}{\delta} \text{Re} \frac{|E|}{\sqrt{E^2 - \tilde{E}_g^2}}. \quad (19)$$

We found the saddle point in the replica-trivial sector of the σ model. This approximation is equivalent to direct calculation of the free energy of the system, averaged over disorder. Indeed, the form of the action (14)

implies that the average partition function obeys the identity $\langle \mathcal{Z}^n \rangle = \langle \mathcal{Z} \rangle^n$. Using this identity and putting the number of replicas to 1, we have for the free energy $\mathcal{F} = -T\langle \log \mathcal{Z} \rangle = -T \log \langle \mathcal{Z} \rangle = T \mathcal{S}|_{n=1}$. Finally, substituting the saddle-point solution θ_ε into the action (14) and noting that the imaginary-time integration simply yields a $1/T$ multiplier in this expression, we find

$$\mathcal{F} = -\frac{1}{\delta} \int \frac{d\varepsilon(\varepsilon + iH)^2}{\sqrt{(\varepsilon + iH)^2 + \tilde{E}_g^2}} + E_0(q). \quad (20)$$

This free energy has the meaning of the Landau-Ginzburg functional while \tilde{E}_g plays the role of the order parameter. The integral in the above expression contains divergent contribution from high energies. As in the standard theory of superconductivity, we get rid of this divergence, subtracting the value of the free energy in the “normal” state, i.e., at $\tilde{E}_g = 0$. Then the result of integration is

$$\begin{aligned} \mathcal{F} - \mathcal{F}_N &= \frac{\tilde{E}_g^2}{\delta} \left[\log \frac{2\Delta}{\Omega(\tilde{E}_g, H)} - \frac{1}{2} \right] \\ &+ \frac{H}{\delta} \left(H - \sqrt{\max^2(\tilde{E}_g, H) - \tilde{E}_g^2} \right) + E_0(q). \end{aligned} \quad (21)$$

The self-consistency equations (15) can be obtained by varying this free energy functional. The solution of Eqs. (15) gives extrema of the free energy; in particular, the trivial solution $\tilde{E}_g = 0$ always satisfies Eqs. (15). We can also estimate fluctuations near the found extremal points. The complete calculation taking into account all possible fluctuating modes including those that break the replica symmetry is cumbersome, but leads to a simple result: the saddle-point approximation is valid provided $\tilde{E}_g \gg \delta$. The details of this calculation for zero magnetic field can be found in Ref. 16, where it was shown that the fluctuations produce a negligible correction to the Josephson current in the Coulomb-blockaded junction between two superconductors via the normal-metallic grain if $\tilde{E}_g \gg \delta$.

III. THERMODYNAMIC MINIGAP

Generally, the system of the self-consistency equations (15) is not analytically solvable. Nevertheless, the ground state energy for the Hamiltonian (11) can be explicitly found in the two limiting cases of small and large q (physically, these limits correspond to the strong and weak Coulomb blockade, respectively). Then Eqs. (15) allow explicit solution.

A. Strong Coulomb Blockade

We start with the case of strong Coulomb blockade. This limit implies $q \ll 1$, which means that the Coulomb energy E_C is much larger than the effective Josephson

energy E_J . The phase K , that is governed by the Hamiltonian (11), is delocalized and strongly fluctuates. At the same time, the charge of the grain is almost fixed. The Coulomb blockade wins the competition versus the proximity effect; the minigap is exponentially suppressed.

At $q \ll 1$, the potential energy in the Hamiltonian (11) can be considered as perturbation. The perturbation theory yields the ground-state energy $E_0(q) = -E_C q^2/2$. Then the self-consistency equations (15) lead to

$$\frac{2E_C\delta}{\tilde{E}_g^2} = \log \frac{2\Delta}{\Omega(\tilde{E}_g, H)}. \quad (22)$$

The quantity $\Omega(\tilde{E}_g, H)$ is defined by Eq. (16) and has different meanings for H below and above \tilde{E}_g . As a result, the equation has two solutions corresponding to these two cases:

$$\tilde{E}_{g0} = 2\Delta \exp(-2E_C\delta/E_g^2) \quad \text{at} \quad H < \tilde{E}_{g0}, \quad (23)$$

$$\tilde{E}_{g1} = \sqrt{\tilde{E}_{g0}(2H - \tilde{E}_{g0})} \quad \text{at} \quad \tilde{E}_{g0}/2 < H < \tilde{E}_{g0}. \quad (24)$$

Note that the conditions for the two branches, $H < \tilde{E}_g(H)$ and $H > \tilde{E}_g(H)$, are rewritten in terms of the fixed value \tilde{E}_{g0} in Eqs. (23) and (24), respectively. The double-valued structure of the whole solution becomes clear in this representation.

One can easily see that \tilde{E}_{g0} corresponds to a local minimum of the free energy (21), while \tilde{E}_{g1} gives a maximum. The “normal” state $\tilde{E}_g = 0$ minimizes the free energy if $H > \tilde{E}_{g0}/2$ and maximizes it otherwise. We introduce notation $H_c^S = \tilde{E}_{g0}$ for the magnetic field of absolute instability of the gapped (S) state. At the field $H_c^N = \tilde{E}_{g0}/2$, the gapless (N) state becomes absolutely unstable. In the interval $H_c^N < H < H_c^S$, the two minima of the free energy coexist. At some value of magnetic field H_c^I lying in this interval the energies of the two states are equal. This is the phase equilibrium point where the first order phase transition occurs. Using the free energy (21), we find this critical field:

$$H_c^I = \frac{\tilde{E}_{g0}}{\sqrt{2}}. \quad (25)$$

The $\tilde{E}_g(H)$ dependence is illustrated in Fig. 1.

The mechanism underlying this first order phase transition is exactly the same as in a bulk ferromagnetic superconductor.¹⁷ The exchange field of the ferromagnet plays the same role as the magnetic field in our case. The correspondence becomes complete if the superconductive pairing constant is taken to be $\lambda = E_g^2/2E_C\delta$ while the Debye cutoff ω_D is replaced by Δ [see Eq. (23)]. The order parameter is \tilde{E}_g . The critical magnetic field, H_c^I , at which the first-order phase transition occurs, is simply the Clogston-Chandrasekhar critical field.¹⁸

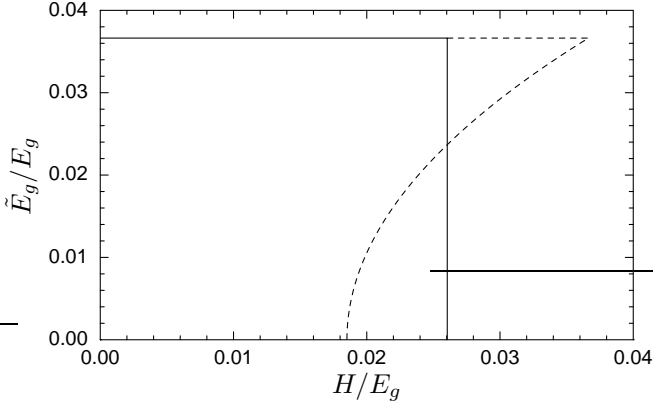


FIG. 1: $\tilde{E}_g(H)$ dependence in the limit of strong Coulomb blockade. Solid line corresponds to the value of \tilde{E}_g that gives the absolute minimum to the free energy. The first order phase transition occurs at $H = H_c^I$, where \tilde{E}_g vanishes abruptly. The dashed line shows other solutions of the self-consistency equations (15). These extra solutions exist only in the interval $H_c^N < H < H_c^S$, where the gapped and gapless states coexist. The curves are plotted for $E_C\delta/E_g^2 = 4.5$. Other parameters are $G = 40$ and $\Delta/E_g = 150$.

B. Weak Coulomb Blockade

Now we turn to the opposite limit of weak Coulomb blockade and large q , which means that the charging energy E_C is much smaller than the effective Josephson energy E_J . The cosine potential in the Hamiltonian (11) strongly localizes the phase K near 0 and π values. At the same time, the fluctuations of charge are strong. The proximity effect wins against the Coulomb blockade and the minigap is only slightly suppressed in comparison with its bare value E_g .

To solve Eqs. (15), we approximate the deep minima of the $\cos 2K$ potential by a one-dimensional oscillator with the ground-state energy $E_0(q) = -2E_C(q - \sqrt{q})$. Then solving Eqs. (15), we find a small correction to the bare minigap:

$$\tilde{E}_g = E_g - \frac{1}{2} \sqrt{\frac{E_C\delta}{\log(2\Delta/\Omega(E_g, H))}}. \quad (26)$$

This dependence is again qualitatively different for magnetic field above and below \tilde{E}_g (approximately equal to E_g). At small magnetic field the minigap does not depend on H . We will denote this value of the minigap by \tilde{E}_{g0} . The state with field-independent minigap is similar to the S state in the strong Coulomb blockade regime. At higher fields \tilde{E}_g is logarithmically diminished. This state will be referred to as S'. More accurate analysis is needed to investigate the vicinity of $H = \tilde{E}_g$ point. It turns out that the first order phase transition found in the opposite limit of strong Coulomb blockade persists. However, now the minigap \tilde{E}_g , being independent of magnetic field at low H , experiences a very small step-like decrease and then gradually diminishes. This is the

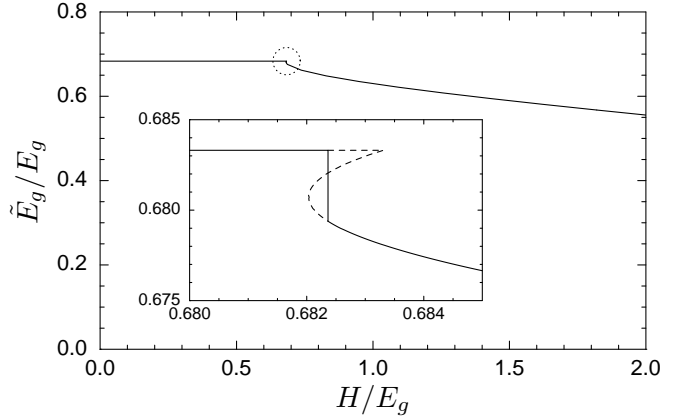


FIG. 2: $\tilde{E}_g(H)$ dependence in the limit of weak Coulomb blockade. The inset is a closeup of the $H = \tilde{E}_{g0}$ point that is encircled in the main plot. As in Fig. 1, the solid line shows the value of \tilde{E}_g that gives the absolute minimum to the free energy, while the dashed line corresponds to extra solutions of the self-consistency equations (15). The curves are plotted for $E_C\delta/E_g^2 = 1.5$. Other parameters are $G = 40$ and $\Delta/E_g = 150$.

first order transition S–S'. The $\tilde{E}_g(H)$ dependence is shown in Fig. 2, where the inset illustrates details near the $H = \tilde{E}_{g0}$ point.

From the free energy (21), we straightforwardly calculate all details of the first order phase transition, that now occurs between two different gapped states, in the limit $q \gg 1$. We omit this bulky calculation and give the results only. The magnetic field H_c^S , at which the S state becomes absolutely unstable is $H_c^S = \tilde{E}_{g0}$. The field of absolute instability of the S' state we denote by $H_c^{S'}$. Along with the critical field H_c^I they are

$$H_c^{S'} = \tilde{E}_{g0} - \frac{E_g}{2}x, \quad H_c^I = \tilde{E}_{g0} - \frac{E_g}{3}x, \quad (27)$$

$$x = \frac{E_C\delta}{16E_g^2 \log^3(2\Delta/E_g)}. \quad (28)$$

The parameter x that determines the scale of the phase coexistence region, is linear in small E_C but contains also an enormously small numerical coefficient. This is the reason why this region is extremely small in Fig. 2.

When the first order transition occurs, the free energy has two minima with identical values. What is the energy barrier between these two minima? This barrier is also numerically very small and equals $2E_g^2x^{3/2}/3\delta$. Obviously, when the height of this barrier becomes comparable with the temperature, fluctuations smear the first order transition. Then a crossover between S and S' states occurs instead of a phase transition.

Finally, when the magnetic field is high enough (beyond the scope of our model), it suppresses the superconductivity in the lead. In the absence of the Coulomb effects, the minigap persists as long as the lead is superconducting, and disappears at the critical field H_{c2} of the

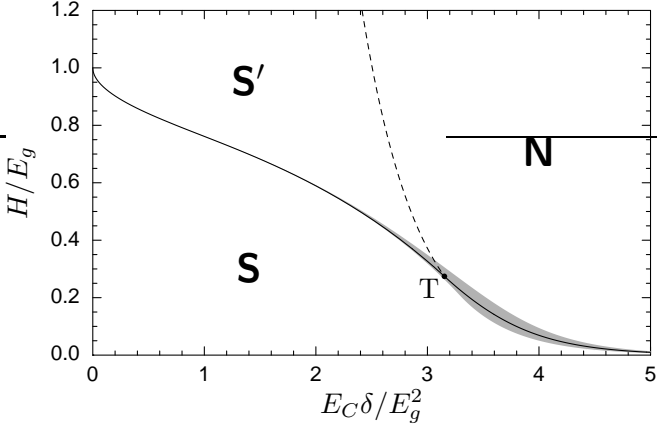


FIG. 3: Phase diagram E_C – H . The solid line marks the first order transition from the S to either N or S' state. The region of phase coexistence is shaded. The dashed line shows the second order S'–N transition. All the three phases equilibrate at the triple point T. A detailed diagram in the vicinity of the triple point is shown in Fig. 4. The diagram is plotted for $G = 40$ and $\Delta/E_g = 150$.

lead. If the weak Coulomb blockade is realized at $H = 0$, then the minigap will vanish at a field slightly smaller than H_{c2} .

C. Intermediate case

In this section we consider an intermediate regime when the Coulomb interaction is comparable with the proximity coupling. In Fig. 3 we present the phase diagram in the E_C – H plane. This diagram covers all limiting regimes considered above along with the intermediate region.

We have already studied the first order transition from S to N and S' states at large and small E_C , respectively. At the same time, the line of absolute instability of the S phase can be extracted from results of Ref. 5 obtained at $H = 0$. Indeed, at low magnetic field $H < \tilde{E}_g$, the self-consistency equations (15) do not contain H . Hence the minigap is independent of the magnetic field (S state) and we use \tilde{E}_{g0} to denote this value of the minigap. The maximal possible magnetic field for this state is $H_c^S = \tilde{E}_{g0}$. Obviously, this result holds for any value of q . The $\tilde{E}_g(E_C)$ dependence in the absence of magnetic field was studied in Ref. 5.

Now we concentrate on the S'–N second order transition and the vicinity of the triple point where all three phases equilibrate. The S'–N transition line can be calculated analytically. Any solution of the self-consistency equations (15) gives an extremum of the free energy: $\partial\mathcal{F}/\partial\tilde{E}_g = 0$. The normal state ($\tilde{E}_g = 0$) always satisfies this condition. The normal state is stable provided $\partial^2\mathcal{F}/\partial\tilde{E}_g^2 > 0$. Calculating the second derivative of the free energy (21) and then taking the limit $\tilde{E}_g \rightarrow 0$, we

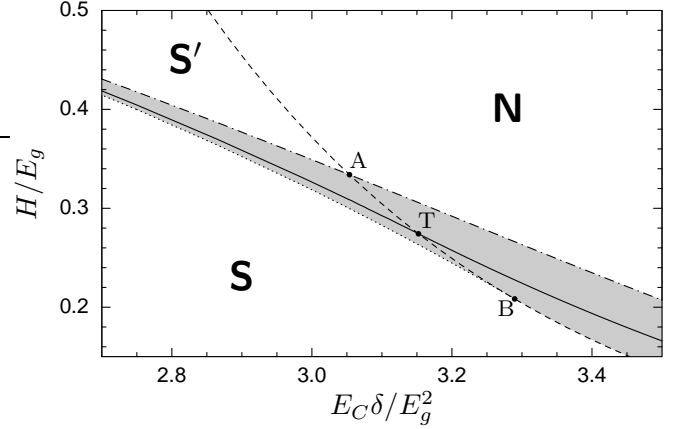


FIG. 4: Phase diagram near the triple point. The solid line shows the first order transition from S to N for E_C above the triple point and from S to S' otherwise. The dashed line corresponds to the critical field H_c^N , given by Eq. (29). The dotted line denotes the absolute instability of the S' phase at the field $H_c^{S'}$. This line ends at the point marked as B. The dash-dotted line is H_c^S . It intersects with H_c^N at the A point. The region of possible metastable state is shaded. The diagram is plotted for $G = 40$ and $\Delta/E_g = 150$.

easily find the critical magnetic field

$$H_c^N = \Delta \exp(-2E_C\delta/E_g^2). \quad (29)$$

This critical field determines the boundary of the normal region in the phase diagram Fig. 3. What happens just below this boundary? The second derivative of the free energy becomes negative. If, at the same time, the fourth derivative is positive, then the free energy achieves a minimum at small \tilde{E}_g . This is the second order phase transition from N to S' state. Otherwise, if the fourth derivative is also negative, then below H_c^N a minimum at \tilde{E}_g vanishes and the only stable state has finite value of the minigap \tilde{E}_{g0} . Thus H_c^N is the normal state absolute instability field for the N–S first order transition. In this case, the critical field (29) coincide with $H_c^N = \tilde{E}_{g0}/2$ that we found in the strong Coulomb interaction limit.

The point on the critical line (29), where the fourth derivative of the free energy changes its sign, is denoted as B (see Fig. 4). To find this point, one should use a more precise value of the ground-state energy of the Hamiltonian (11) taking into account the fourth order perturbation correction: $E_0(q) = E_C(-q^2/2 + 7q^4/128)$. Then taking the fourth derivative of the free energy (21), we find the equation $H_B^2 = E_g^4/7E_C\delta$, which, together with Eq. (29), determines the position of the B point.

In Fig. 4 the closeup of the triple point region is shown. The H_c^N curve is shown by the dashed line. The line of absolute instability of the S' phase $H_c^{S'}$ (the dotted line in Fig. 4) ends in the B point. Indeed, the S' phase with arbitrary small \tilde{E}_g exists only if the fourth derivative of the free energy is positive. Another feature of the phase diagram, the A point, is the point where the N–

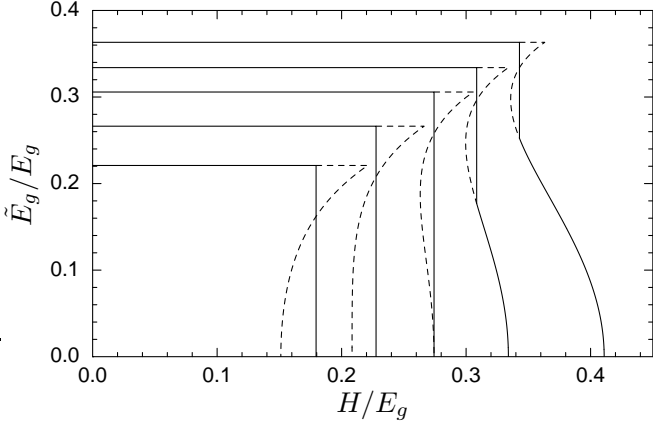


FIG. 5: Minigap as a function of magnetic field (solid lines) for several values of E_C near the triple point. The dashed lines shows extra solutions of the self-consistency equations (15). The curves from left to right correspond to $E_C\delta/E_g^2 = 3.45, 3.289$ (B point), 3.152 (T point), 3.054 (A point), and 2.95. The other parameters are $G = 40$ and $\Delta/E_g = 150$.

S' second order transition and the absolute instability of the S phase occur simultaneously. Finally, between the A and B points on the H_c^N line, the triple point T lies. This is the point where the first and second order transition lines intersect. All the three phases have the same energy in this point.

Another illustration of the complicated phases structure near the triple point is given by Fig. 5, where several $\tilde{E}_g(H)$ dependences are shown. The leftmost curve corresponds to E_C above the B point. Qualitatively, this case is similar to the strong Coulomb blockade limit (see Fig. 1). The next curve is plotted for E_C taken at the B point. It looks much the same, but $\tilde{E}_g(H)$ (dashed line) vanishes as the fourth rather than square root of the magnetic field. The next curve is for the T point. The first and second order transitions (solid and dashed lines) occur at the same magnetic field. The right but one curve is for the A point ($H_c^N = \tilde{E}_{g0}$). The rightmost curve illustrates the case of E_C below the A point. It is similar to the weak interaction limit (see Fig. 2). The minigap vanishes continuously at H_c^N . As E_C further decreases, this critical field grows exponentially and rapidly goes beyond the scope of our model.

IV. TUNNELING DENSITY OF STATES

Measuring the thermodynamic density of states is experimentally complicated due to small size of the sample. The tunneling technique is more practical in this case. The actual measured quantity is the tunnel current which depends on the voltage applied between the system and a normal-metallic external tip. The differential conductance dI/dV extracted from this experiment is proportional to the local *tunneling* density of states at

energy eV . The latter is determined by the imaginary part of the one-particle Green function. Without interaction, the thermodynamic and tunneling DOS coincide. However, in an interacting system the Green function is “dressed” by the interaction that yields the difference between the two quantities. In the σ -model language, the thermodynamic DOS is determined by the \tilde{Q} matrix, see Eq. (17), while the tunneling DOS is given by a similar expression with the “dressed” matrix Q .

In fact, the differential conductance gives the tunneling density of states only at zero temperature. If $T > 0$, the tunneling electrons are dispersed in the energy range of the order of T . The expression for dI/dV then reads

$$\frac{dI}{dV} = \frac{\delta}{2R_T} \int dE \frac{\rho^{\text{tun}}(E + eV)}{4T \cosh^2(E/2T)}, \quad (30)$$

with R_T being the tunnel resistance between the tip and the grain. In order to measure the subtle structure of the tunneling DOS due to the Zeeman splitting, the temperature should be low enough:

$$T \ll \min\{\tilde{E}_g, H\}. \quad (31)$$

To calculate the TDOS for one spin projection (spin up), we should analytically continue the expression

$$\begin{aligned} \rho_{\uparrow}^{\text{tun}}(\varepsilon) &= \frac{1}{\delta} \text{tr} \langle \hat{\tau}_3 Q_{\varepsilon\varepsilon} \rangle \\ &= \frac{1}{\delta} \int_{-\infty}^{\infty} d\tau e^{i\varepsilon\tau} \text{tr} \left\langle \hat{\tau}_3 e^{i\hat{\tau}_3 K_\tau} \tilde{Q}_{\tau 0} e^{-i\hat{\tau}_3 K_0} \right\rangle \end{aligned} \quad (32)$$

to the real energies, $i\varepsilon \rightarrow E + i0$, and take its real part. The angle brackets denote averaging with weight $e^{-S[\tilde{Q}, K]}$ where the action is given by Eq. (9). The TDOS for the spin down is then obtained after inverting the sign of the magnetic field. The adiabatic and saddle-point approximations allow to substitute \tilde{Q} of the form (10) and average over K . This procedure leads to the expression

$$\rho_{\uparrow}^{\text{tun}}(\varepsilon) = \frac{2}{\delta} \int_{-\infty}^{\infty} \frac{d\omega}{2\pi} \frac{(\omega + iH)}{\sqrt{(\omega + iH)^2 + \tilde{E}_g^2}} C(\varepsilon - \omega), \quad (33)$$

where $C(\omega)$ is the phase correlator containing average over the ground state of the Hamiltonian (11):

$$C(\omega) = \int_{-\infty}^{\infty} d\tau e^{i\omega\tau} \langle \cos(K_\tau - K_0) \rangle. \quad (34)$$

This quantity can be expressed in terms of the eigenvalues E_n and the eigenfunctions $|n\rangle$ of the Hamiltonian (11):

$$C(\omega) = \sum_n P_n \frac{2A_n}{\omega^2 + A_n^2}, \quad A_n = E_n - E_0, \quad (35)$$

$$P_n = |\langle 0 | \cos K | n \rangle|^2 + |\langle 0 | \sin K | n \rangle|^2. \quad (36)$$

Now we can perform the analytic continuation to real energies in Eq. (33). In Fig. 6 we plot the integration

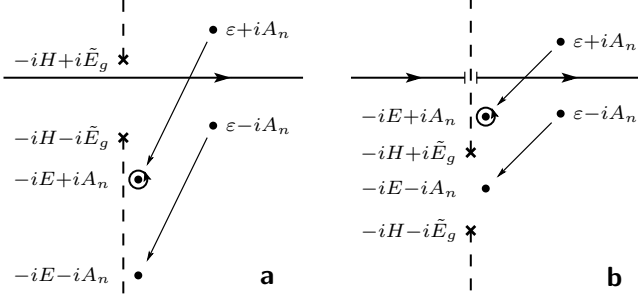


FIG. 6: Analytic continuation of the integrand of Eq. (33) in the complex ω plane. The integral is taken along the real axis denoted by the line with arrow. The dashed lines are branch-cut discontinuities. The small dots show the poles of the n th term in the sum (35) for $C(\varepsilon - \omega)$. These poles move to new positions at the imaginary axis due to the analytic continuation. The residue in the pole that traversed the real axis provides the real part of the integral and determines the TDOS. (a) Left panel corresponds to the S phase, $H < \tilde{E}_g$. The Coulomb and proximity gaps add up around $E = 0$. (b) Right panel corresponds to the S' phase, $H > \tilde{E}_g$, where the two gaps are separated.

contour in the complex plain of the ω variable and show the two poles of $C(\varepsilon - \omega)$ along with the branch cut for the rest of the integrand. For simplicity we retain only a pair of poles corresponding to the n th term of the sum (35). The analytic continuation moves the poles; as a result, all the singularities of the integrand reside on the imaginary axis. Therefore the integral along the real axis becomes purely imaginary and does not contribute to the TDOS. The real part, and hence the TDOS, is nonzero if a pole traverses the real axis while moving (see Fig. 6). Then the residue in this pole will determine the result. Note, that the value of this residue is nothing but the thermodynamic DOS at the energy corresponding to the final position of the pole. To obtain the complete expression for the TDOS, we sum the contributions from all the terms in the sum (35) and symmetrize the result with respect to the spin direction:

$$\begin{aligned} \rho^{\text{tun}}(E) &= \frac{1}{2} [\rho_{\uparrow}^{\text{tun}}(E) + \rho_{\downarrow}^{\text{tun}}(E)] \\ &= \sum_n P_n \vartheta(|E| - A_n) \rho(|E| - A_n). \end{aligned} \quad (37)$$

Here $\vartheta(x)$ is the Heaviside step function and $\rho(E)$ is the thermodynamic DOS given by Eq. (18).

The resulting expression for the TDOS has a clear physical meaning. Every term of the sum (37) is obtained from $\rho(E)$ by inserting the $2A_n = 2(E_n - E_0)$ Coulomb gap around $E = 0$ and multiplying by the factor P_n . The energy dependence of the TDOS is qualitatively different for the two gapped phases, S and S', described in the previous section. In the S phase, when $H < \tilde{E}_g$, the peaks of the TDOS (see Fig. 7) are split due to the Zeeman effect, but the whole picture resembles the result of Ref. 5.

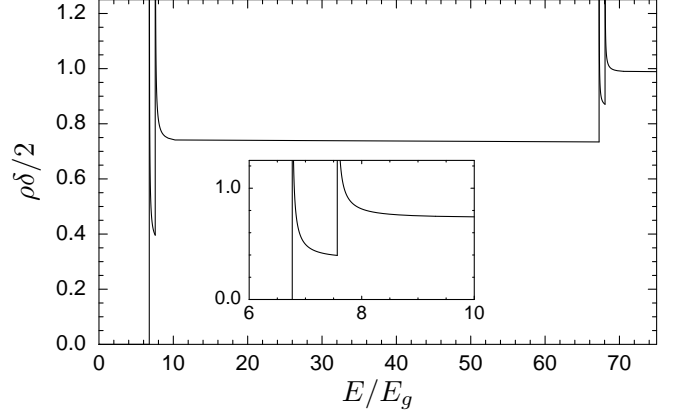


FIG. 7: Energy dependence of the tunneling DOS for the S phase. The parameters are $E_C\delta/E_g^2 = 2.5$, $H/\tilde{E}_g = 0.4$, and $\Delta/E_g = 150$. The inset shows the details of the Zeeman splitting of the first peak. The second peak is split in the same manner.

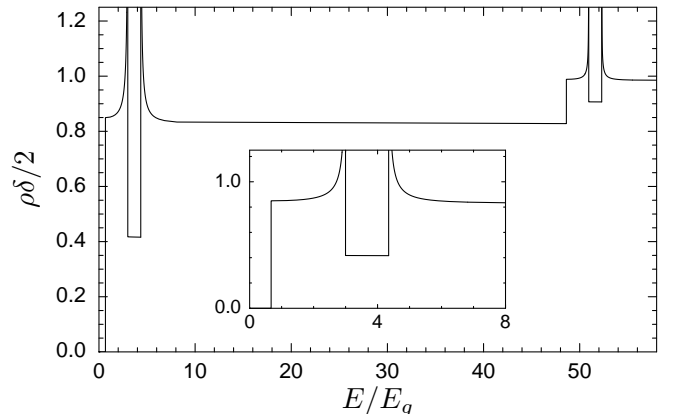


FIG. 8: Energy dependence of the tunneling DOS for the S' phase. The parameters are $E_C\delta/E_g^2 = 1.0$, $H/\tilde{E}_g = 3.0$, and $\Delta/E_g = 150$. The inset shows the details of the first peak structure. The Coulomb and proximity gap are clearly separated for $H > \tilde{E}_g$.

At higher magnetic field, $H > \tilde{E}_g$, the grain is in the S' phase. The Coulomb and proximity gaps are now separated as shown in Fig. 8. The Coulomb gap is always centered around $E = 0$ while the minigap is shifted by H . The density of states inside this shifted minigap is no longer zero due to the contribution from electrons with the opposite spin.

The resulting expression (37) contains the matrix elements P_n and the energy level separations $A_n = E_n - E_0$. Both quantities can be found analytically in the limits of weak and strong Coulomb interaction. Previously, we have mentioned two symmetries of the Hamiltonian (11): it commutes with operations $K \mapsto -K$ and $K \mapsto K + \pi$. Therefore, the P_n coefficients are nonzero only for $n = 4k + 1$ and $n = 4k + 2$. Another their property is the normalization, $\sum_n P_n = 1$, thus

$\rho(E) = \rho^{\text{tun}}(E) = 2/\delta$ if the energy E is far from the Fermi energy. The sequence P_n rapidly decreases at any strength of the Coulomb interaction. This allows us to keep only $n = 1$ and $n = 2$ terms in the sum (37). In the weak Coulomb blockade limit, $q \gg 1$, we approximate the $\cos 2K$ potential by two deep parabolic wells. The splitting of the two lowest levels is exponentially small. To the main order in $1/\sqrt{q}$, we have

$$P_1 = 1 - \frac{1}{4\sqrt{q}}, \quad P_2 = \frac{1}{4\sqrt{q}}, \quad (38)$$

$$A_1 = 0, \quad A_2 = 4E_C\sqrt{q}. \quad (39)$$

In the opposite case of strong Coulomb interaction, $q \ll 1$, we employ the perturbation theory in q and obtain

$$P_{1,2} = \frac{1}{2} \left(1 \pm \frac{q}{2} \right), \quad A_{1,2} = E_C(1 \mp q). \quad (40)$$

In the limit of strong Coulomb interaction, at high magnetic fields $H > H_c^1$, the minigap is absent and the grain is in the N phase. In this case, the TDOS exhibits the pure Coulomb gap at energies below E_C and is constant above this gap: $\rho^{\text{tun}}(E) = (2/\delta)\vartheta(|E| - E_C)$. In fact, even in the N regime a very small minigap of the order of $\sqrt{\delta/H}\tilde{E}_{g0}$ [where \tilde{E}_{g0} , given by Eq. (23), is the minigap at $H = 0$] persists in the TDOS due to the fluctuations, that we neglected in this paper. The mechanism of this effect is similar to that for a superconductive grain in a strong magnetic field described in Ref. 19.

V. CONCLUSIONS

In conclusion, we developed the self-consistent theory for proximity and charging effects in the presence of ex-

ternal magnetic field. The minigap induced in the grain shows complicated dependence on magnetic field. Two distinct minigapped states exist, and the first order phase transition occurs between them. Transition to the gapless state is of the first order from S state and of the second order from S'. The tunneling DOS is also different in S and S' states. In high magnetic field, $H > \tilde{E}_g$, TDOS acquires two distinct gaps: Coulomb gap at zero energy and proximity minigap shifted from zero by magnetic field.

The systems discussed in this paper can be experimentally realized at the following parameters: the grain can be made of a noble metal and have a form of disk with thickness $d \sim 25$ nm and diameter an order of magnitude larger. At the interface transparency of order 2×10^{-6} (insulating oxide barrier) we estimate $\delta \sim 5 \times 10^{-4}$ K, $E_g \sim 0.01$ K, $E_C \sim 0.1$ K, $E_J \sim 1$ K, and $G \sim 100$. The lead can be made of Nb, then $\Delta \sim 12$ K and the magnetic fields should be smaller than 1 T.

VI. ACKNOWLEDGEMENTS

We are grateful to I. S. Beloborodov, A. V. Lopatin, and V. M. Vinokur for useful discussions. This research was supported by the RFBR grants Nos. 04-02-16348 and 04-02-08159, the Russian Ministry of Education and Science under the contract RI-112/001/417, the program “Quantum Macrophysics” of the Russian Academy of Sciences. P.M.O. and Ya.V.F. also acknowledge the support from the Dynasty foundation. Ya.V.F. was also supported by the RF Presidential Grant No. MK-3811.2005.2, the Russian Science Support Foundation, CRDF, and the Russian Ministry of Education and Science.

* Electronic address: ostrov@itp.ac.ru

† Electronic address: fominov@landau.ac.ru

‡ Electronic address: feigel@landau.ac.ru

¹ W. Belzig, F. K. Wilhelm, C. Bruder, G. Schön, and A. D. Zaikin, *Superlattices Microstruct.* **25**, 1251 (1999).

² *Single Charge Tunneling*, edited by H. Grabert and M. H. Devoret (Plenum, New York, 1992).

³ X. Wang and H. Grabert, *Phys. Rev. B* **53**, 12621 (1996).

⁴ K. A. Matveev and L. I. Glazman, *Phys. Rev. Lett.* **81**, 3739 (1998).

⁵ P. M. Ostrovsky, M. A. Skvortsov, and M. V. Feigel'man, *Phys. Rev. Lett.* **92**, 176805 (2004).

⁶ A. A. Golubov and M. Yu. Kupriyanov, *Zh. Éksp. Teor. Fiz.* **96**, 1420 (1989) [Sov. Phys. JETP **69**, 805 (1989)].

⁷ A. I. Larkin and Yu. N. Ovchinnikov, *Phys. Rev. B* **28**, 6281 (1983).

⁸ V. Ambegaokar and A. Baratoff, *Phys. Rev. Lett.* **10**, 486 (1963).

⁹ A. M. Finkel'stein, in *Soviet Scientific Reviews*, edited by I. M. Khalatnikov (Harwood Academic Publishers GmbH,

London, 1990), Vol. 14.

¹⁰ J. W. Negele and H. Orland, *Quantum Many-Particle Systems* (Perseus Books, Boulder, 1988).

¹¹ K. B. Efetov, *Supersymmetry in Disorder and Chaos* (Cambridge University Press, Cambridge, 1996).

¹² A. Kamenev and A. Andreev, *Phys. Rev. B* **60**, 2218 (1999).

¹³ D. V. Averin and Yu. V. Nazarov, *Phys. Rev. Lett.* **69**, 1993 (1992); *Physica B* **203**, 310 (1994).

¹⁴ K. B. Efetov and A. Tschersich, *Phys. Rev. B* **67**, 174205 (2003).

¹⁵ K. D. Usadel, *Phys. Rev. Lett.* **25**, 507 (1970).

¹⁶ P. M. Ostrovsky and M. V. Feigel'man, *Pis'ma Zh. Éksp. Teor. Fiz.* **82**, 863 (2005) [JETP Lett. **82**, 763 (2005)].

¹⁷ G. Sarma, *J. Phys. Chem. Solids* **24**, 1029 (1963).

¹⁸ A. M. Clogston, *Phys. Rev. Lett.* **9**, 266 (1962); B. S. Chandrasekhar, *Appl. Phys. Lett.* **1**, 7 (1962).

¹⁹ H.-Y. Kee, I. L. Aleiner, and B. L. Altshuler, *Phys. Rev. B* **58**, 5757 (1998).